Full Length Article

In situ photogenerated defects on surface-complex BiOCl (0 1 0) with high visible-light photocatalytic activity: A probe to disclose the charge transfer in BiOCl (0 1 0)/surface-complex system

Sunxian Weng[a], Jun Hu[a], Meiliang Lu[a], Xinxin Ye[a], Zengxia Pei[a], Mianli Huang[a], Liyan Xie[b], Sen Lin[a], Ping Liu[a,*]

[a] Research Institute of Photocatalysis, State Key Laboratory of Photocatalysis on Energy and Environment, College of Chemistry and Chemical Engineering, Fuzhou University, Fuzhou 350002, PR China
[b] Department of environment and biological engineering, Putian University, Putian 351100, PR China

ABSTRACT

Surface functional modification through small organic molecules to form surface complex which possess unique electronic and optical properties, is a hopeful strategy in activating BiOCl-0 1 0 for visible light harvesting. However, the significant charge transfer between surface complex and BiOCl-0 1 0 in photocatalytic process is vague. In this work, we ingeniously design a facile repeat experiment to obtain reliable information on charge transfer mechanisms and structure-reactivity relationships between surface complex and BiOCl-0 1 0 under reaction condition. Interestingly, this charge transfer gives rise to the formation of defects which are protected by a disordered outer layer on surface. Moreover, the introduction of defects plays a vital role in photocatalytic and photoelectric performance, which can be verified by DFT calculations. Our current work is expected to offer new insight into charge transfer between surface complex and substrates for better understanding to photocatalytic reactions and for rational design and synthesis of photocatalyst with high activity.

© 2014 Elsevier B.V. All rights reserved.

1. Introduction

Photocatalysis is a promising process for the utilization of solar energy by storing photon energy in chemical bonds which has been diffusely used to alleviate the energy crisis by splitting water for hydrogen production utilizing light energy [1–4] and mitigate the environment deterioration established by poisonous pollutants [5,6]. Over the past several years, BiOCl as an important ternary compound semiconductor has attracted scientific interest as a promising photocatalyst in environmental application because of the coexistence of unique and excellent electrical, magnetic, optical and luminescent properties [6–9]. However, the photoconversion efficiency of BiOCl is still far from satisfaction owing to the rapid recombination of photogenerated excitons and the indigent harvest of visible light. Therefore, it is imperative to tailor BiOCl materials in a suitable manner to enhance photoconversion efficiency.

As is known to us, catalytic reactions always occur on the surface of catalysts relying on their surface microstructure (e.g. morphologies, atom arrangement, active sites and electronic structure). Surface microstructure control engineering has been a subject of intensive research because the chemical, optical, electrical, and magnetic properties of materials surface can be allowed to tailor, thus enhancing their scientific and technological applications [10–17]. For instance, the combination of photocatalysts with metal nanoparticles or organic dyes such as Au or ruthenium–bipyridyl complexes is effective for obtaining the sensitivity to visible light [10,17]. However, due to the high costs of these precious metals which are difficult employed in practical application, some other approaches with similar properties should be proposed as alternatives. Recently, surface functional embellishing by small organic molecules to form surface complex which possesses unique optical and electronic properties, is a powerful approach in activating wide band gap photocatalysts for visible light harvesting owing to their low cost, easy recycle and relatively high visible light photocatalytic performances [15,18]. Stimulated by this strategy, the degradation of 2-naphthol by facet-dependent BiOCl based on surface complex under visible light irradiation has

been reported previously.[19] The electron excitations approach of surface complex is reasonably expounded by a well-known charge-transfer-complex approach between the organic molecule and metal site on the semiconductor surface. However, the significant charge transfer between surface complex and BiOCl-0 1 0 is vague. The development of this technology has been required to gain a much better fundamental understanding to the nature of charge transfer process between surface complex and semiconductors.

In our study on BiOCl-0 1 0/surface complex system reported here, it is found that the introduction of surface complex with the charge transfer process drives a reconstruction of BiOCl surface structure, resulting in the formation of defects. The defects, a kind of surface states, steadily exist on the surface owing to the protection of a disordered outer layer formed by surface complex [20–22]. The synergy between the defect state and the surface complex effectively improves the photocatalytic activities of BiOCl-0 1 0. DFT calculations are also performed to interpret the enhancement of visible-light absorption induced by the defects. Moreover, the relative mechanism is proposed. Our current work is expected to offer new insight into charge transfer between surface complex and substrates for better understanding to photocatalytic reactions and for rational design and synthesis of photocatalyst with high activity.

2. Experimental

2.1. Preparation

2.1.1. Materials

KCl, Bi(NO$_3$)$_3$·5H$_2$O, NaOH, 2-naphthol (2-NAP), 1-naphthol (1-NAP), 2,3-dihydroxynaphthalene (2,3-DN) and acetonitrile were purchased by Sinopharm Chemical Reagent Co. Deionized water was used throughout this study. 5,5-Dimethyl-1-pyrroline N-oxide (DMPO) was used as radicals spin trap and obtained from Alfa Aesar. Other commercial chemicals were of analytical reagent grade without further purification.

2.1.2. Material synthesis

BiOCl nanosheets with dominant exposed (0 1 0) facets were fabricated via an early reported approach [19]. In this synthesis, 1 mmol KCl and 1 mmol Bi(NO$_3$)$_3$·5H$_2$O were dissolved in 19 cm^{-3} deionized water at room temperature. Then, 1 M NaOH solution was transferred into the mixture to monitor the pH-value of solution to approximate 6. The obtained mixture solution was vigorously stirred for 1 h and then transferred into a 28 cm^{-3} Teflon liner stainless auto-clave. The auto-clave was allowed to be heated up to 160 °C and kept at 160 °C for 24 h under spontaneous pressure. Then the auto-clave was cooled to room temperature in the air. The obtained products were rinsed using deionized water and ethanol for several times. Finally, the products were dried at 80 °C oven for 12 h in the air in order to wipe off water and ethanol. The obtained products were denoted as BiOCl-(0 1 0).

BiOCl-010-used was synthesized as follows: 80 mg BiOCl-0 1 0 was dispersed to 80 ml with 2.0 × 10^{-5} M 2-NAP solution (solvent: H$_2$O-acetonitrile = 9999/1 v/v) for 1 hour visible light irradiation ($\lambda \geq$ 420 nm). In addition, the product was obtained under the similar condition without the addition of light irradiation was denoted as S-BiOCl-0 1 0. And the formation of surface complex on S-BiOCl-0 1 0 had been confirmed according to previous report [19]. The obtained products were also gathered and rinsed with deionized water and ethanol several times. Finally, the resulting products were moved to an 80 °C oven for 12 h.

2.2. Material characterization

The morphologies of the BiOCl-0 1 0 were performed by a field-emission scanning electron microscope (SEM) (FEI Nova NanoSEM-230). The optical absorption properties of the samples were analyzed using the ultraviolet–visible diffuse reflectance spectroscopy (UV–vis DRS) with an ultraviolet–visible spectrophotometer (Lambda 950, PerkinElmer Co.). BaSO$_4$ acted as the background. The XRD patterns of products were recorded on a Bruker D8 X-ray diffractometer via Cu$_{K\alpha}$ radiation operated at 40,000 V and 0.04 A. A Bruker model A300 spectrometer was used to investigate the electron spin resonance (ESR) signals of samples. The settings of ESR were as follows: microwave power, 6.35 mW; frequency, 9.86 GHz; center field, 3512.48 G. The Raman spectra were obtained using a Renishaw system equipped with a 50× microscope objective lens. A green laser beam (λ = 532 nm) was utilized for excitation. The FTIR data were recorded using a nicolet Nexus-670 FTIR spectrophotometer with a resolution of 4 cm^{-1}. The photoluminescence (PL) spectra were collected using a Varian Cary-Eclipse-500 with an excitation wavelength at 320 nm. XPS characterization was collected by an ESCALAB 250 photoelectron spectroscope system. The photoelectrochemical measurement was similar to previous report [8]. The BAS Epsilon workstation was utilized to monitor the photocurrents of samples. The electrochemical impedance spectroscopy (EIS) was performed on a ZENNIUM electrochemical workstation (Zahner, Germany). HPLC–mass spectrometry (HPLC–MS) identification of intermediate products is performed using a Thermo ACCELA equipped TSQ Quantum ACCESS MAX mass spectrometry detector. The HPLC was fitted with an Agilent Eclipse XDB-C18, 4.6 × 150 mm, 5 μm. The mobile phase is composed of acetonitrile and doubly distilled water. The v/v ratio CH$_3$CN/H$_2$O is 80/20 and the flow rate is 0.3 ml/min. The MS detection is performed with electrospray ionization in negative mode.

2.3. Photocatalytic activity measurements

The photodegradation of 2-NAP were used to evaluate the photocatalytic activities of the samples under visible light irradiation. Typically, 0.08 g samples were added to 80 cm [3] 2 × 10^{-5} mol/L 2-NAP solution in a quartz container. The suspensions would be stirred in darkness for 60 min prior to illumination toward establish the adsorption–desorption equilibrium. During the procedure of photodegradation, 3 cm[3] suspensions were collected per 20 min and the concentration of 2-NAP was detected using an ultraviolet–visible spectrophotometer (Varian Cary-50) after centrifuged. A TOC-VCPH analyzer (Shimadzu Co.) was used to analyze the total organic carbon (TOC) of the degradation.

2.4. DFT calculations

All calculations were carried out based on the periodic DFT calculations by using the Vienna *ab initio* simulation package (VASP) [23–25] with the gradient-corrected PW91 exchange-correction functional [26]. For valence electrons a plane-wave basis set was employed with a cut-off of 550 eV and the ionic cores were described with the projector augmented-wave (PAW) method [27,28]. A 3 × 3 × 1 Monkhorst-Pack k-point grid was adopted to sample the Brillouin zone. [29]

The optimized bulk lattice parameter a and c/a ratio for bulk BiOCl was found to be 3.91 Å and 2.015, in agreement with the previous report. [30] We chose (0 1 0) facet as the model since it was found to be dominant in our synthesized BiOCl crystal. The slab consisted of five layers and all atoms were allowed to relax in our calculations. A vacuum spacing was set to be 14 Å to avoid inter-layer interactions. In order to explore how photogenerated
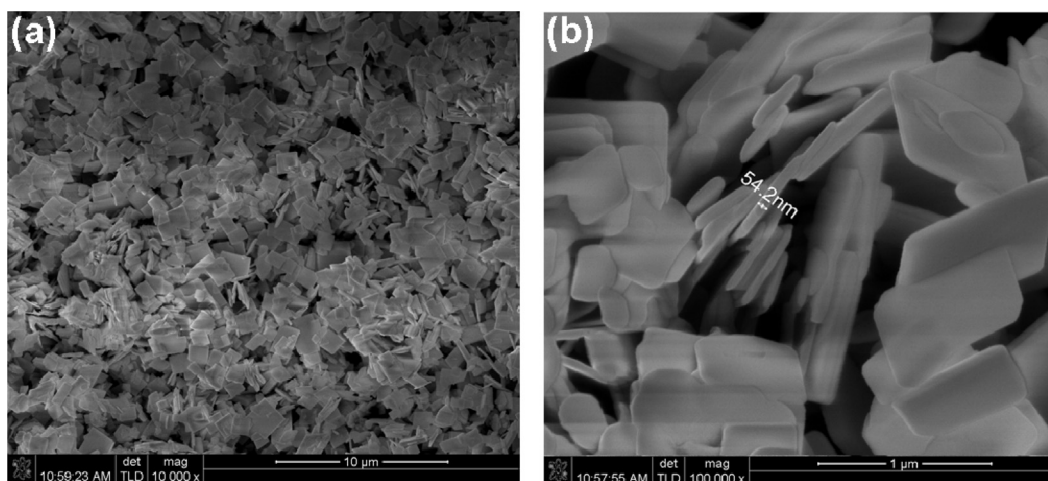
Fig. 1. SEM (a) Low magnification and (b) high magnification SEM images of the as-synthesized BiOCl-0 1 0 nanosheets.

defects affect the optical properties of BiOCl (0 1 0), three BiOCl (0 1 0) surfaces with 0, 1 and 2 electron defects were adopted.

The optical absorption coefficient (α_{abs}) was deduced by converting the complex dielectric function obtained directly from the VASP calculations according to the following Eq. (1):

$$\alpha_{abs} = \frac{2\sqrt{2}\pi}{\lambda_0}\left(\sqrt{\varepsilon_1^2 + \varepsilon_2^2} - \varepsilon_2^2\right)^{\frac{1}{2}} \tag{1}$$

Where ε_1 and ε_2 are the real and imaginary parts of frequency dependent complex dielectric constant, respectively, and λ_0 is the wavelength at a corresponding frequency. [31]

3. Results and discussion

BiOCl nanosheets exposing (0 1 0) facets are prepared via a simple hydrothermal method [19]. As shown in Fig. 1, the typical SEM images reveal that the BiOCl-0 1 0 is present in tetragonal nanosheets of ca. 20–80 nm thickness and 200–1000 nm width. In addition, we have previously reported the as-prepared BiOCl nanosheets are covered with dominant (0 1 0) facets [19]. Theoretical and experimental research have demonstrated that in contrast to BiOCl (0 0 1) surface, the surface of BiOCl (0 1 0) consists of more terminal bismuth atoms rather than terminal oxygen atoms, and these terminal bismuth structures can serve as active sites for photocatalytic reactions [6]. Thus the as-synthesized BiOCl nanosheets with exposed (0 1 0) facets is highly desirable for catalytic reactions.

In our experiments, the photoactivity of the BiOCl-0 1 0 and BiOCl-0 1 0-used is evaluated through the degradation of 2-NAP. It is evident that the photocatalytic activities of BiOCl-0 1 0 present an enhancement trend during the experiments repeatedly for three times (Fig. 2). The common explanation for this phenomenon is the formation of new compounds or defects. Fig. 3 presents the XRD patterns of the BiOCl-0 1 0, BiOCl-0 1 0-used and BiOCl-0 1 0-2-run-used. It is interesting to note that for all samples, the diffraction patterns are almost the same and exhibit characteristic diffraction peaks ascribed to BiOCl tetragonal crystals. No characteristic peaks of any other phases and impurities are observed, indicating that the crystalline structure of the BiOCl-0 1 0 nanosheets does not change after photocatalytic reaction. The 2-NAP molecules attached to BiOCl-0 1 0 surface or BiOCl-0 1 0-used is via a naphtholate linkage based on FTIR data [19]. Moreover, no new FTIR peaks (Fig. 4) are observed on BiOCl-0 1 0-used compared with S-BiOCl-0 1 0, indicating that the photo-degradation of 2-NAP does not cause the formation of polymeric deposits [19,32]. Furthermore, the extent of mineralization is evaluated by measuring the total organic
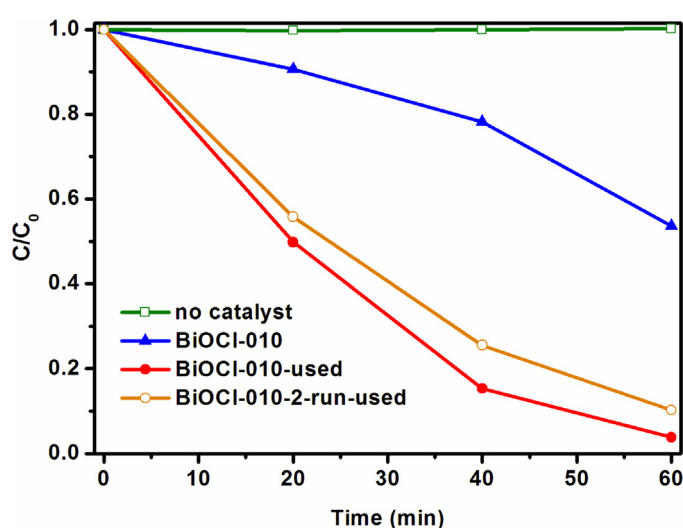

Fig. 2. Time profiles of photocatalytic degradation of 2-NAP over samples under visible light irradiation.
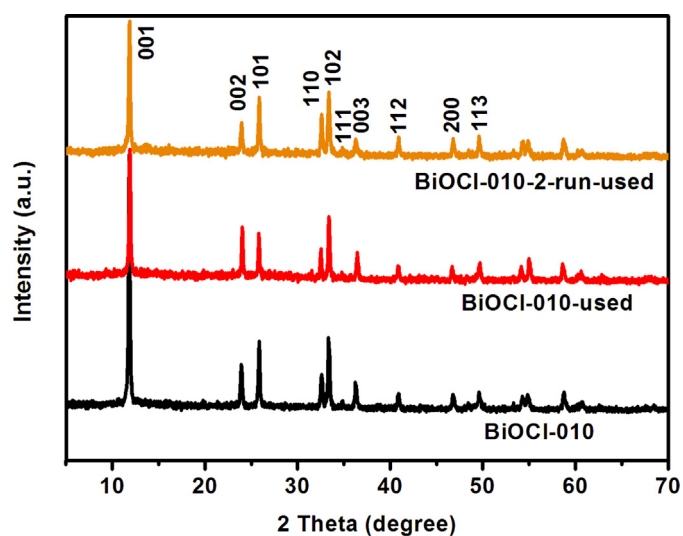

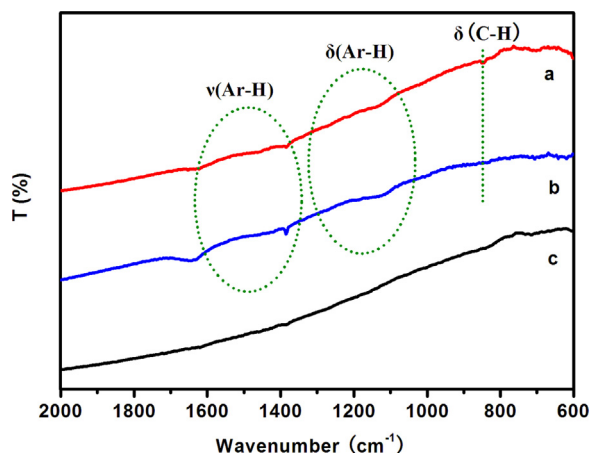**Fig. 3.** XRD patterns of the BiOCl-(0 1 0), BiOCl-010-used and BiOCl-010-2-run-used.

Fig. 4. FT-IR spectra for (a) BiOCl-0 1 0-used, (b) S–BiOCl-0 1 0 and (c) BiOCl-0 1 0.

Fig. 6. Calculated absorption spectra for the BiOCl-0 1 0 surface with and without electron defects.

carbon (TOC). The initial total organic carbon of 2-NAP is 9.05 mg L^{-1}. After visible light irradiation for 60 min, the TOC value of the final solution for BiOCl-0 1 0-used is 4.32 mg L^{-1}, whereas it is 6.28 mg L^{-1} for BiOCl-0 1 0. The corresponding mineralization efficiency is evaluated to be ca. 52.3% for BiOCl-0 1 0-used and 30.6% for BiOCl-0 1 0. The principal conclusion from the XRD and FTIR result is that the increased activity is most likely arose from the surface defects rather than new compounds. In fact, the rate of C/C_0 over BiOCl-0 1 0 is accelerated with photoirradiation time, implying that the formation of surface defects at the beginning of reaction.

It has been well known that surface defects always impact the optical property of photocatalysts [33]. The UV–vis diffused reflectance (DRS) absorption spectra are used to examine the optical absorption of the original and used catalysts, as shown in Fig. 5. For all samples, there are three typical absorption bands below 370 nm corresponding to the band gap energy of BiOCl. With respect to BiOCl-0 1 0, S–BiOCl-0 1 0 has a new extra consecutive visible light absorption region from 400 to 800 nm due to the absorption of surface complex in the visible light region. As expected, defects can further enhance the harvesting of visible light and narrow the band gap of BiOCl-0 1 0-used which can be clearly found by optical absorption curves and the tangent slop line, [33] suggesting that it will possess a higher photocatalytic activity for target reactions. This observation can be interpreted by DFT calculations. As shown in Fig. 6, we can see that the calculated absorption spectra for the (0 1 0) surface with only one electron defect are very similar to that without electron defects in the range
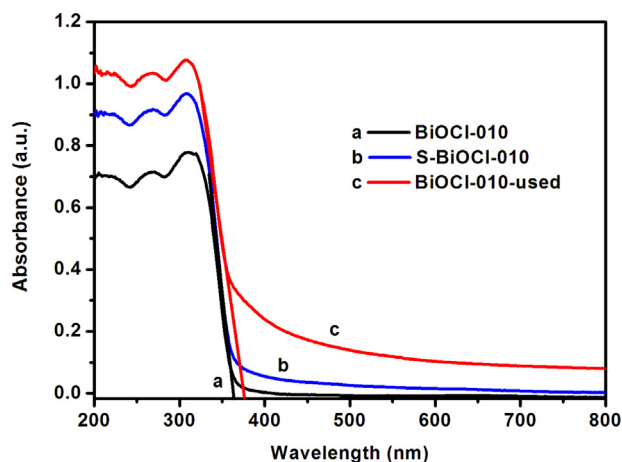

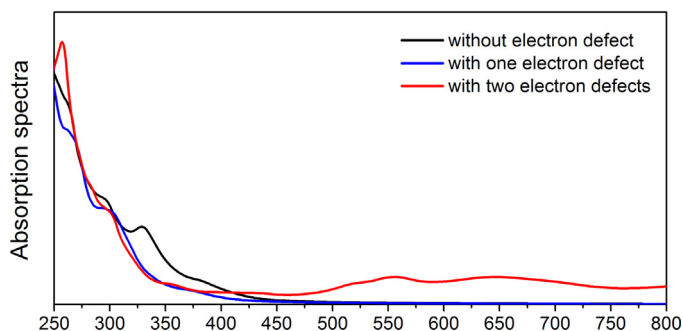**Fig. 5.** UV–visible DRS and spectra of BiOCl-0 1 0, S–BiOCl-0 1 0 and BiOCl-0 1 0-used.

of 400–800 nm. Interestingly, after two electron defects were considered in the (0 1 0) surface, the absorption of visible-light was found to be significantly enhanced. Therefore, it is believed that at least two electron defects are required in the surface system to shift the spectral response into the visible region and improve the photocatalytic performance. This hypothesis has been verified via the degradation of 2-NAP, 1-NAP (Fig. S1) and 2, 3-DN (Fig. S2) and photocurrents over the samples under the same conditions. The determination of defect species is vital for disclosing the charge transfer behaviors between surface complex and BiOCl-0 1 0.

The electron spin resonance (ESR) technology is a common and powerful tool to examine and determinate the unpaired electron species (e.g. free radicals and oxygen vacancy) in materials. Fig. 7a a depicts the ESR spectra of the samples measured at room temperature in the darkness. No ESR signal is observed in BiOCl-0 1 0 and S–BiOCl-0 1 0 in the dark. In contrast, a symmetrical and sharp peak at $g = 2.004$ in BiOCl-0 1 0-used is obviously observed under the same experimental conditions. This g-value of 2.004 should be assigned to Bi^{3+}—$O\bullet^-$—Bi^{3+} according to similar report in TiO_2 [13,34]. The introduction of defect states generally changes the surface properties (e.g. optical property, electronic property) of BiOCl-0 1 0. For optical property, defect states can draw impurity level into BiOCl-0 1 0 to narrow its band gap for harvesting more visible light even obtaining visible light response. This significant change of optical and photocatalytic property has been confirmed by DRS, photoactivities and photocurrents. On the other hand, defect sites are presumed to affect the electron–hole recombination process in photocatalysts, causing a change in chemical reaction rates that relies on charge transfer from either holes or electrons. [35] In general, surface defects are very unstable and readily removed under common circumstances or in aqueous media. To our surprise, the ESR signal of BiOCl-0 1 0-used does not disappear after two months (Fig. 7b), indicating that the defects state is very stable in ambient conditions. It suggests that a protective cover presumably exists on the surface of BiOCl-0 1 0 to protect Bi^{3+}—$O\bullet^-$—Bi^{3+}. The protective layer is most likely due to the surface reconstruction induced by surface complex. This hypothesis has been confirmed by Raman spectroscopy measurement.

The evidence of the protective layer has been investigated and proved by analyzing the Raman spectroscopy which acted as effective means to distinguish the surface structural change of materials. In Fig. 8, one weak band and three distinguished bands are observed in the Raman spectra for all samples. The weak band at 398 cm^{-1} assigned to B_{1g} and E_g band is originated from the motion of O atoms. The three strong peaks at 60 cm^{-1} (external-A_{1g}), 146 cm^{-1} (A_{1g}) and 201 cm^{-1} (E_g) belong to inherent Bi—Cl stretching mode in BiOCl-0 1 0 [8,19]. As compared to BiOCl-0 1 0, the S–BiOCl-0 1 0 shows a fire-new band at 500–1700 cm^{-1} in Fig. 8. However, these new Raman peaks cannot belong to BiOCl or 2-NAP, implying that structural changes most likely due to Raman selection rule is broken
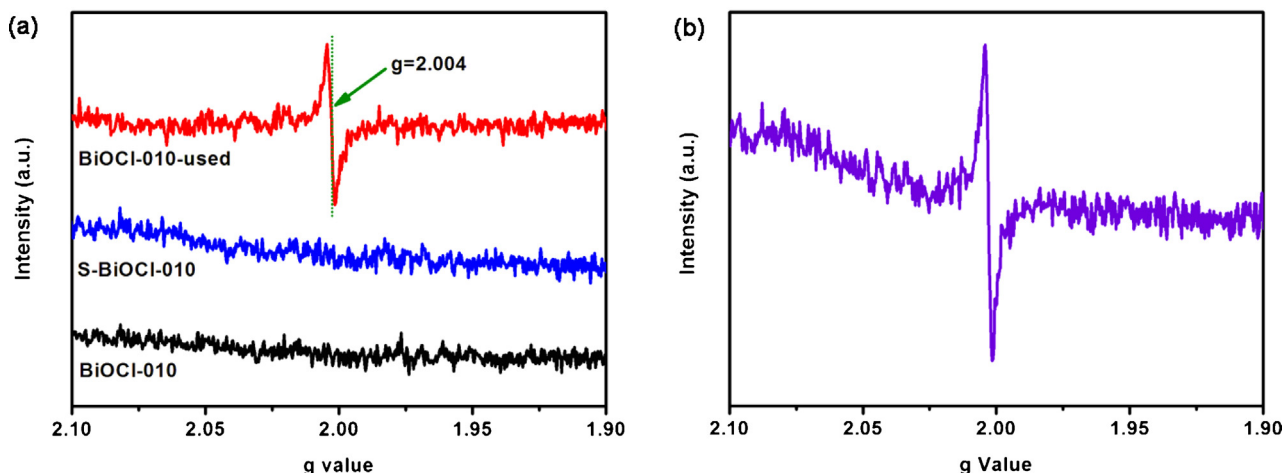
Fig. 7. ESR spectra of (a) BiOCl-0 1 0, S-BiOCl-0 1 0 and BiOCl-0 1 0-used and (b) BiOCl-0 1 0-used after 2 month under normal ambient conditions.
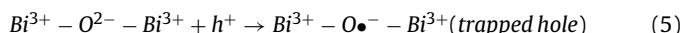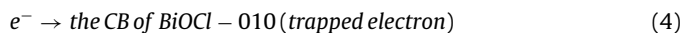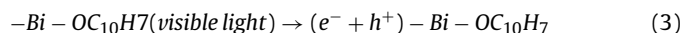
down by surface structure reconstruction with the formation of surface complex [1]. This surface structure reconstruction will provide a protective layer to protect the surface defects [36]. The similar occurrence is found in BiOCl-0 1 0-used, manifesting that the surface defects can be effectively protected via the surface structure reconstruction. Moreover, the evidence of existence of surface complex on BiOCl-0 1 0-used surface is further proved by analyzing the XPS spectrogram of the C (1s), O (1s) and Bi (4f) core level, as displayed in Fig. 9 [19]. The C 1s peak at ca. 284.6 eV results from the surface adventitious carbon in BiOCl-0 1 0. The C 1s spectra of the S-BiOCl-0 1 0 and BiOCl-0 1 0-used (Fig. 9a) can be deconvoluted into three peaks corresponding to C—C/C=C, C—H, and C—O with binding energies of 284.6 eV, 286.1 eV, and 288.5 eV for the S-BiOCl-010, and 284.6 eV, 286.0 eV, and 288.5 eV for the BiOCl-0 1 0-used [37,38]. Obviously, the surface carbon enrichment in S-BiOCl-0 1 0 and BiOCl-0 1 0-used could be attributed to the presence of 2-NAP. O 1s core level spectra of BiOCl-0 1 0 can be best fitted into 3 peaks while the S-BiOCl-0 1 0 and BiOCl-0 1 0-used have 4 curves (Fig. 9b). The band located at binding energies of 530.0 ± 0.1 eV is attributed to oxygen in the BiOCl crystal lattice [39]. The higher peak at some 532.6 ± 0.1 eV relates to chemisorbed or dissociated oxygen species on the surface of BiOCl, such as adsorbed H_2O and/or O_2 [40]. A medium binding energy component, centered at 531.3 ± 0.1 eV, is generally originated from the presence of hydroxyl group on the surface of the BiOCl-010 [39]. The additional O 1s peak of S-BiOCl-0 1 0 and BiOCl-0 1 0-used is found at 533.5 ± 0.1 eV, corresponding

well to the value reported in the literature for phenolic oxygen group [41]. Something significant to note here is the increase of phenolic oxygen group (0–17.8%-12.5%), together with remarkable decrease of —OH (21.1%–14.9%-16.0%) comparing results of BiOCl-0 1 0 to S-BiOCl-0 1 0 and BiOCl-0 1 0-used. This result confirms that 2-NAP is linked to BiOCl-0 1 0 surface via the dehydration reaction as shown as following Eq. (2).

$$-Bi-OH + HO-C_{10}H_7 = -Bi-O-C_{10}H_7 + H_2O \qquad (2)$$
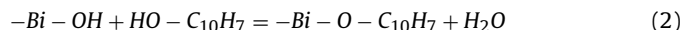
The two characteristic bands of energies located in 158.9 eV and 164.2 eV assigned to the spin orbital splitting photoelectrons of Bi ($4f_{7/2}$) and Bi ($4f_{5/2}$) in the BiOCl are found in BiOCl-0 1 0, S-BiOCl-0 1 0 and BiOCl-0 1 0-used (Fig. 9c). The other two high binding energies peaks located in 159.8 eV (Bi ($4f_{7/2}$)) and 165.2 eV (Bi ($4f_{5/2}$)) are observed in S-BiOCl-0 1 0 and BiOCl-0 1 0-used and attributed to the formation of Bi—O—C bond through a naphtholate linkage. In addition, Bi atom or low valence states of bismuth ion is not detected in the S-BiOCl-0 1 0-used via Raman or XPS, possibly due to the electrons in CB from photoinduced surface complex fast separated to solution instead of the reduction from Bi^{3+} to Bi [8,42]. Interestingly, the band of the motion of the oxygen atoms located at approximately 396 cm^{-1} does not disappear in the Raman spectra of BiOCl-0 1 0-used, illuminating that no oxygen vacancy is generated after photocatalytic reaction [42]. No oxygen vacancy further corroborate the presence of Bi^{3+}—$O\bullet^-$—Bi^{3+} species. These experiment consequences confirm the distinguishing surface structures between BiOCl-0 1 0 and BiOCl-0 1 0-used.

On the basis of above results and discussions, we specify the following charge transfer paths in surface-complex/BiOCl-010. The surface complex is excited by absorbing visible light to generate reduced electron and oxidized substance (denoted as hole), the electron is transferred into the CB of BiOCl-0 1 0, while the hole is used to generate Bi^{3+}—$O\bullet^-$—Bi^{3+}.

$$-Bi-OC_{10}H7(visible\ light) \rightarrow (e^- + h^+) - Bi - OC_{10}H_7 \qquad (3)$$

$$e^- \rightarrow the\ CB\ of\ BiOCl-010\ (trapped\ electron) \qquad (4)$$

$$Bi^{3+}-O^{2-}-Bi^{3+} + h^+ \rightarrow Bi^{3+}-O\bullet^- - Bi^{3+}(trapped\ hole) \qquad (5)$$

To further confirm that the BiOCl-0 1 0-used with defects have stronger capacity in visible light absorption, the transient photocurrents are carried out to distinguish the changes of photoelectrochemical responses and verify the formation and transfer of electrons in materials. Because of the wide band gap, the photocurrent response of the BiOCl-0 1 0 electrode is negligible under the visible light irradiation. In contrast, the S-BiOCl-0 1 0 (Fig. 10)
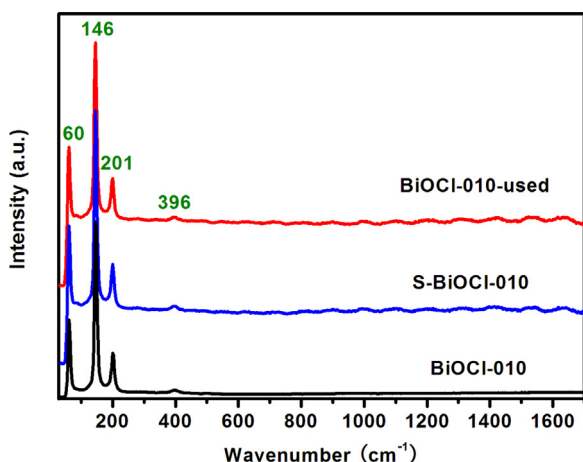

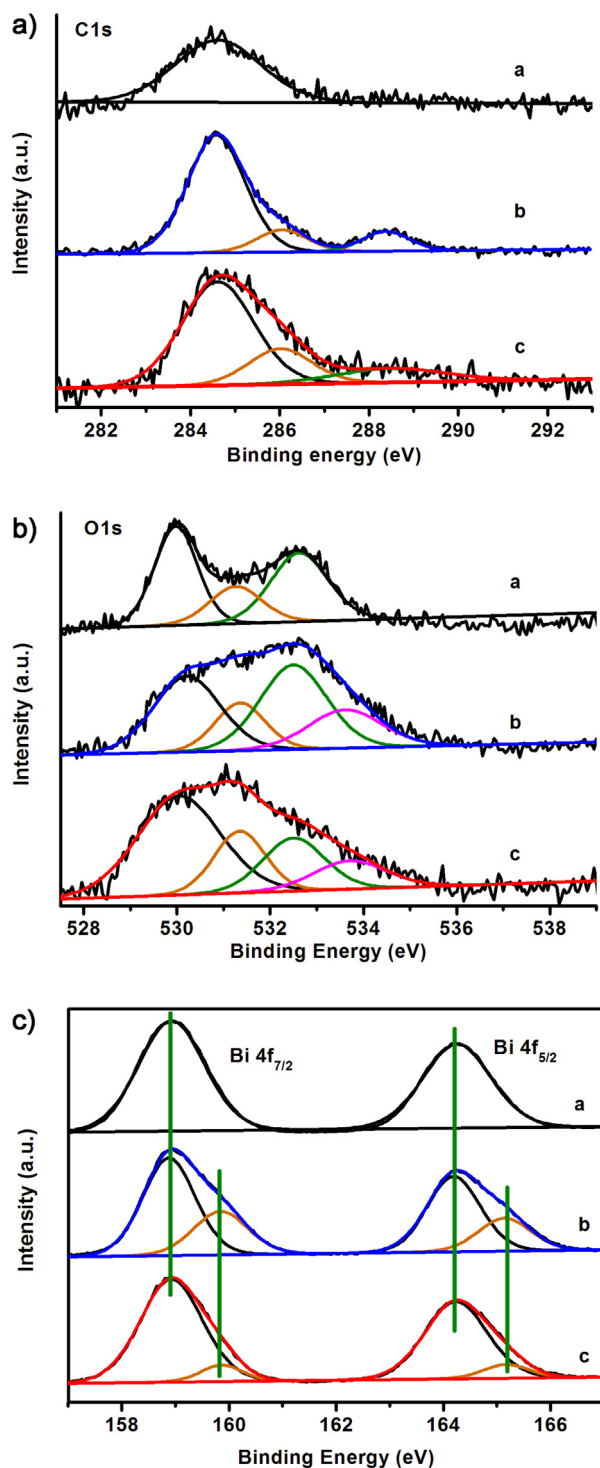**Fig. 8.** Raman spectra of BiOCl-0 1 0, S-BiOCl-0 1 0 and BiOCl-0 1 0-used.

Fig. 9. (a) C 1s, (b) O 1s and (c) Bi 4f X-ray photoelectron spectroscopy spectra of (a) BiOCl-0 1 0, (b) S-BiOCl-0 1 0 and (c) BiOCl-0 1 0-used.

Fig. 10. Transient photocurrent responses of the samples in 0.2 M Na$_2$SO$_4$ with 0 mV bias versus Ag/AgCl electrodes at visible light illumination.

the band gap of BiOCl-0 1 0 and thus leading to visible light response. Moreover, the photocurrents of S-BiOCl-0 1 0 disappear immediately after extinguishment of illumination, while BiOCl-0 1 0-used still exhibits a residual photocurrent. The relatively slower decay of the photocurrents may result from fast charge transfer with a prolonged lifetime.

The electrochemical impedance spectroscopy (EIS) technique is widely utilized for the study of the interfacial charge transfer properties in electrode/electrolyte and the effective lifetime of electrons. The EIS measurement is carried out covering the frequency from 4 MHz to 50 mHz intervals using an amplitude of 10 mV with zero bias vs. Ag/AgCl. Fig. 11a displays the typical EIS plots of the as-synthesized BiOCl-0 1 0, S-BiOCl-0 1 0 and BiOCl-0 1 0-used in darkness, which is presented as Nyquist plots. The diameter of the semicircle is equal to the resistance of electron transfer and the semicircle at high frequency is characteristic process of electron transfer [43]. It can be obviously observed from Fig. 11a that the arc for S-BiOCl-0 1 0 is smaller than bare BiOCl-0 1 0. This result shows that the surface complex especially naphthalene ring is able to enhance the electron mobility. Meanwhile, the sequence of EIS is accordance with the order of their photocurrent strength. As depicted, the BiOCl-0 1 0-used exhibits the lowest arch as compared to S-BiOCl-0 1 0 and BiOCl-0 1 0, elucidating that the defects also significantly facilitate the interfacial charge transfer. In addition, effective lifetime of electrons (τ) in BiOCl-0 1 0 conduction band can be estimated by relation as follows: $\tau \approx 1/(2\pi f)$, where f is the inverse minimum frequency [44]. From this equation, the electron lifetime of BiOCl-0 1 0-used (1.528 µs) is calculated approximately 1.5 times and 2 times higher than that of the S-BiOCl-0 1 0 (0.968 µs) and BiOCl-0 1 0 (0.771 µs), respectively (Fig. 11b). This prolonged lifetime should be attributed to fast charge transfer which can effectively suppress the recombination of charge and enhance the photoconversion efficiency. The lower recombination of charge will be deeply confirmed by photoluminescence measure.

Photoluminescence (PL) emission is diffusely used to disclose the separation efficiency of the photo-excited holes and electrons for semiconductors because the recombination of holes and electrons will cause the PL emission signal. As presented in Fig. 12, the PL spectra of the samples exhibit an emission band at 340–425 nm under the excitation at 320 nm at room temperature. The emission band at 362 nm is assigned to absorption band edge of BiOCl. As is known to us, the lower recombination rate of photogenerated electrons and holes is generally indicative of the lower PL intensity. Obviously, the S-BiOCl-0 1 0 and BiOCl-0 1 0-used show markedly subdued PL intensity relative to the bare BiOCl-010, indicating an

exhibits a distinct visible light photocurrent. This distinct photocurrent can be attributed to the excited electrons from surface complex migrated to ITO glass via charge-transfer-complex pathway. More interestingly, the BiOCl-0 1 0-used shows an enhanced visible light photocurrent which ca. 7.5-fold increase than that of S-BiOCl-0 1 0 which is good accordance with photocatalytic activity. The accounts of this tremendous enhancement are attributed to the synergy between surface complex and defects. The photocurrent results once more verify that the defects can narrow
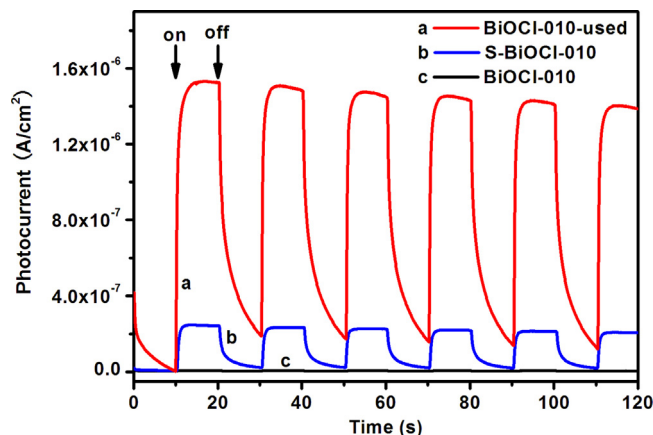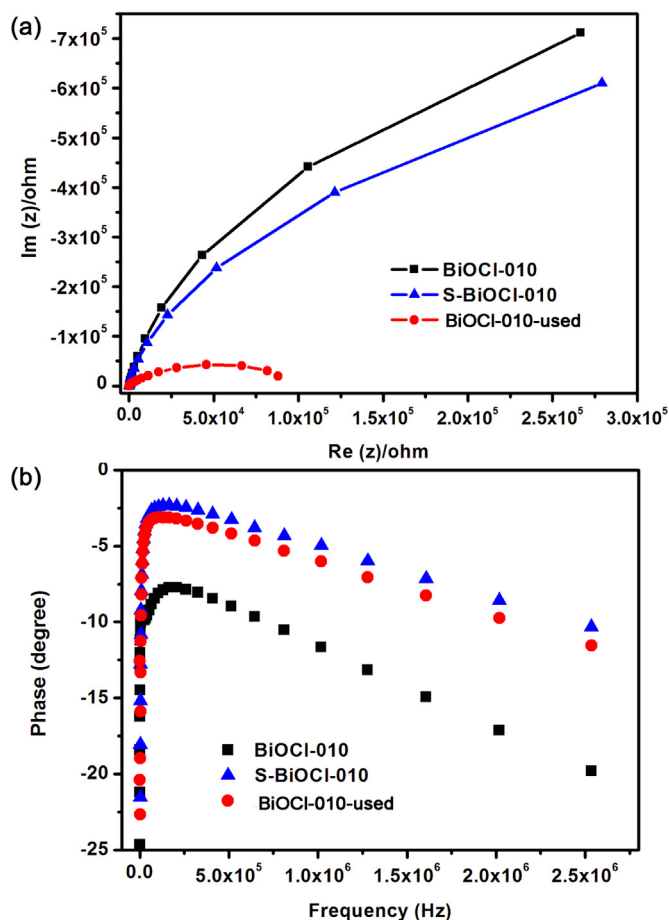
Fig. 11. (a) Nyquist impedance plots of BiOCl-0 1 0, S-BiOCl-0 1 0 and DS-BiOCl-0 1 0 in 0.2 M Na$_2$SO$_4$ with 0 mV bias versus Ag/AgCl electrodes (b) the corresponding Bode-phase of three electrodes.

excellent decline in charges recombination. This conclusion of PL is good agreement with that of EIS.

The intermediate products formed in the photocatalytic degradation of 2-naphthol in the aqueous BiOCl-0 1 0 and BiOCl-0 1 0-uesd suspension for 60 min are investigated by HPLC–MS analysis. For BiOCl-0 1 0 (Fig. S5), two peaks are identified and their retention times are 4.40 min and 6.31 min, respectively. The other intermediates are not identified because of their low concentration in the reaction mixture. The retention time at 6.31 shows a
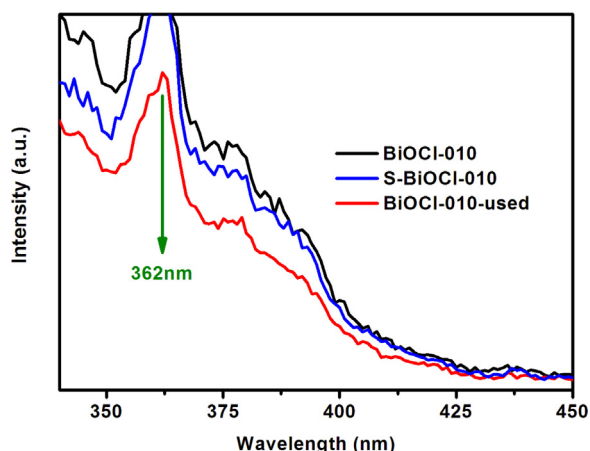

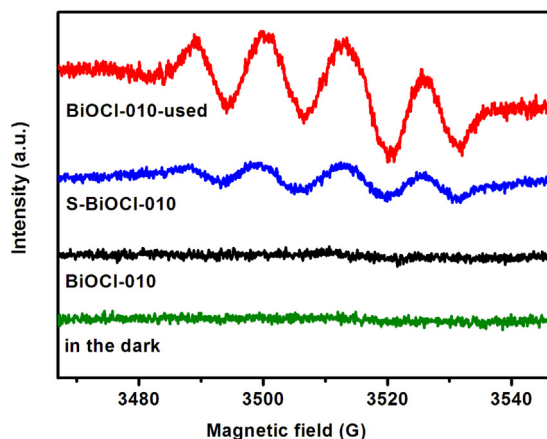**Fig. 12.** Photoluminescent spectra of BiOCl-0 1 0, S-BiOCl-0 1 0 and BiOCl-0 1 0-used.

Fig. 13. The DMPO-O$_2$•- adducts are detected for the samples dispersion in methanol.

strongest mass peak (m/z = 144) which is attributed to 2-NAP. The other obtained main fragment (m/z = 164) at t_r = 4.40 indicates the intermediate product most likely is 2-hydroxycinamic acid which is confirmed by several researches [45,46]. This result manifests that the opening of an aromatic cycle is the major route of transformation. With respect to BiOCl-0 1 0, only one peak (t_r = 4.40) is found in BiOCl-0 1 0-used (Fig. S8) due to the rapid degradation of 2-NAP in BiOCl-0 1 0-used under the visible light irradiation. However, the important reaction process is that involving an oxidizing species which can attack and transform the organic molecules through the formation of intermediates having progressively higher oxygen to carbon ratios.

In order to understand influence of defects on the reactive oxygen species, the ESR technique is utilized to detect them in different solution by the addition of radical scavenger (DMPO). The reactive oxygen species, such as strong oxidizing hydroxyl radicals (•OH) and weak oxidizing superoxide radicals (O$_2$•$^-$), are generally involved in photodegradation of organic pollutants in solution [5,47]. The •OH and O$_2$•$^-$ are probed in water-medium and methanol-medium, respectively. The typical characteristic bands of the DMPO-O$_2$•$^-$ adducts are both detected over S-BiOCl-0 1 0 and BiOCl-0 1 0-used in the methanol-medium under the irradiation of visible light, as shown in Fig. 13. No ESR signals are observed in darkness, elucidating that the visible light is essential factor for the generation of O$_2$•$^-$. The ESR signal intensity of the DMPO-O$_2$•$^-$ adducts on BiOCl-0 1 0-used is obviously stronger than that of S-BiOCl-0 1 0. This increase intensity should be owed to the introduction of the defects which draw impurity level into band gap of BiOCl-0 1 0 and thus can be excited by visible light to generate more charge carriers. According to previous work, the ESR signal of DMPO-•OH adducts on S-BiOCl-0 1 0 is not observed with or without visible light irradiation. To our surprise, the BiOCl-0 1 0-used exhibits a weak ESR signal bands of DMPO-•OH adducts under the irradiation of visible light (Fig. 14). This exciting experimental phenomenon further confirms the assumption of narrowing BiOCl-0 1 0 via the introduction of defects which can be excited by visible light to generate electron–hole pairs. Additionally, the other ESR signal peaks can be assigned to DMPO-O$_2$•$^-$ adducts, suggesting that the superoxide radicals plays an important role toward the degradation of 2-NAP on BiOCl-0 1 0-used. To further confirm the impact of O$_2$•$^-$ radical species on degradation of 2-NAP over BiOCl-0 1 0-used, the controlled experiments under N$_2$-saturated conditions have been performed (Fig. 15). The remarkably decreased rate for degradation of 2-NAP over BiOCl-0 1 0-used under N$_2$-saturated conditions is in favor of the hypothesis.

A tentative mechanism for the photochemical processes is depicted in Fig. 16. Under the visible light illumination, the
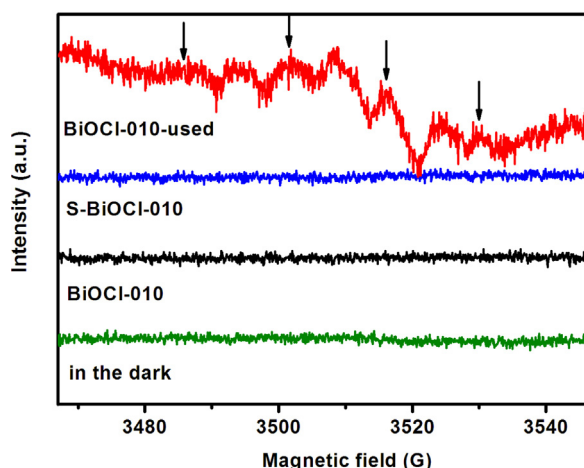
Fig. 14. The DMPO-•OH adducts are detected for the samples dispersion in water.

surface complex can be excited to generate main species (electrons) via charge-transfer-complex pathway. And the electrons are meteorically shifted from surface complex to the conduction band of BiOCl-0 1 0. In addition, the introduction of defects can narrow the band gap of BiOCl-0 1 0 via increasing the valence band (VB) energy level result in enhancing the harvesting and response of visible light. Then, the narrowing BiOCl-0 1 0 can be excited by visible light, thus the electron–hole pairs will be generated. The electrons in the CB of BiOCl-0 1 0 will be transferred to molecular oxygen, an electron acceptor, to form main active oxygen species $O_2\bullet^-$. The formation of •OH is mainly derived from the H_2O by trapping the holes from the impurity energy level. Subsequently, these formed active oxygen species trigger the oxidative degradation reaction of 2-NAP.

It is essential to make a scientific conclusion for the crucial effect of defects ($O\bullet^-$) on BiOCl-0 1 0 with superior photocatalytic performance enhancement based on the above results and discussions. (1) The visible light absorption intensity is further improved and effectively utilized owing to the presence of defects via drawing an impurity level into band gap of BiOCl-0 1 0 to reach harvesting and response of visible light. (2) The introduction of defects can boost the interfacial charge transfer, thus effectively reducing recombination rate of photo-generated electrons–holes. (3) On account of the disordered layer coating induced by surface complex, the defects
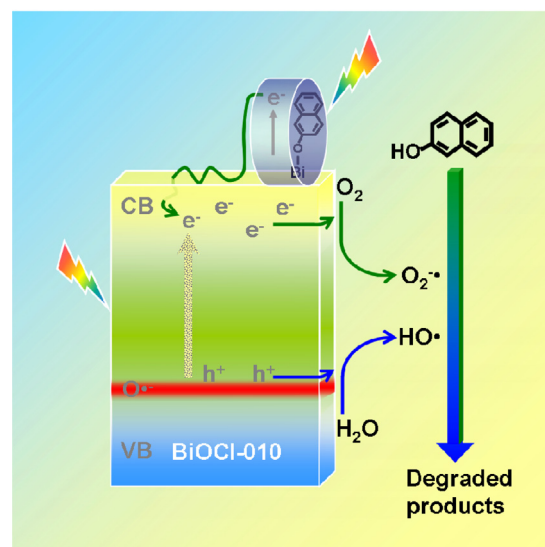

Fig. 15. Photocatalytic degradation of 2-NAP in the presence of N_2 under visible light irradiation over BiOCl-0 1 0-used.

Fig. 16. Proposed mechanisms for the photo-oxidation of 2-NAP over BiOCl-0 1 0-used under the visible light VB = valence band, CB = conduction band, h$^+$ = hole, e$^-$ = electron.

can be perfectly protected and stably exist under normal ambient conditions. In sum, these integrative factors can cause the markedly increased photoactivity of BiOCl-0 1 0-used.

4. Conclusions

In summary, we have developed a facile one-step method for the production of stable defects on BiOCl-0 1 0 surface via visible-light-driven surface complex under ambient conditions. A feasible charge transfer mechanism between BiOCl-0 1 0 and surface complex is proposed and able to commendably account for the generation of defects. And, the defects are stable on BiOCl-0 1 0 surface due to the disordered protected layer coating induced via the surface complex. The introduction of defects can enhance the visible-light absorption, boost the interfacial charge transfer and prolong the lifetime of electron. The cooperative effect of these beneficial properties can further improve the photocatalytic performance of the degradation of 2-NAP under visible light illumination. These findings will deepen our comprehending of photocatalytic reactions involving surface complex and may offer a reasonable strategy and synthesis of wide band gap photocatalysts with high visible light absorption and response.

Appendix A. Supplementary data

Supplementary data associated with this article can be found, in the online version, at http://dx.doi.org/10.1016/j.apcatb.2014.07.051.

References

[1] X. Chen, L. Liu, P.Y. Yu, S.S. Mao, Science 331 (2011) 746–750.
[2] X. Chen, S. Shen, L. Guo, S.S. Mao, Chem. Rev. 110 (2010) 6503–6570.
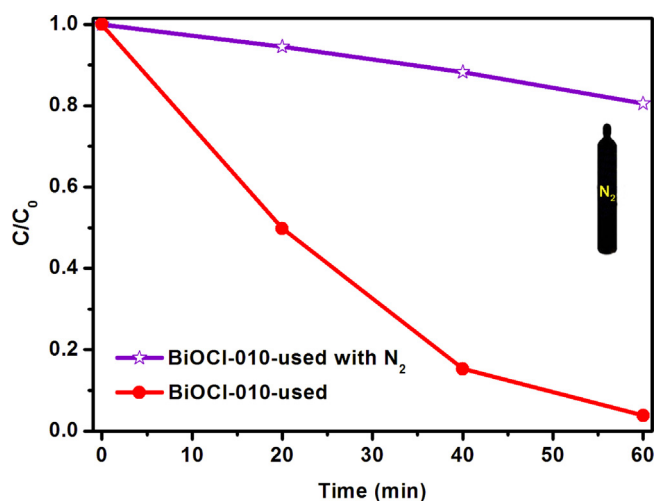[3] F. Zuo, L. Wang, T. Wu, Z. Zhang, D. Borchardt, P. Feng, J. Am. Chem. Soc. 132 (2010) 11856–11857.

[4] G. Liu, L.-C. Yin, J. Wang, P. Niu, C. Zhen, Y. Xie, H.-M. Cheng, Energ. Environ. Sci. 5 (2012) 9603–9610.
[5] M.R. Hoffmann, S.T. Martin, W. Choi, D.W. Bahnemann, Chem. Rev. 95 (1995) 69–96.
[6] J. Jiang, K. Zhao, X. Xiao, L. Zhang, J. Am. Chem. Soc. 134 (2012) 4473–4476.
[7] L. Ye, L. Zan, L. Tian, T. Peng, J. Zhang, Chem. Commun. 47 (2011) 6951–6953.
[8] S. Weng, B. Chen, L. Xie, Z. Zheng, P. Liu, J. Mater. Chem. A 1 (2013) 3068–3075.
[9] D.H. Wang, G.Q. Gao, Y.W. Zhang, L.S. Zhou, A.W. Xu, W. Chen, Nanoscale 4 (2012) 7780–7785.
[10] Y. Tian, T. Tatsuma, J. Am. Chem. Soc. 127 (2005) 7632–7637.
[11] S. Linic, P. Christopher, D.B. Ingram, Nat. Mater. 10 (2011) 911–921.
[12] R. Su, R. Tiruvalam, Q. He, N. Dimitratos, L. Kesavan, C. Hammond, J.A. Lopez-Sanchez, R. Bechstein, C.J. Kiely, G.J. Hutchings, F. Besenbacher, ACS Nano 6 (2012) 6284–6292.
[13] J.B. Priebe, M. Karnahl, H. Junge, M. Beller, D. Hollmann, A. Bruckner (Eds.), Angew. Chem. Int. 52 (2013) 11420–11424.
[14] S. Kim, W. Choi, J. Phys. Chem. B 109 (2005) 5143–5149.
[15] T. Kamegawa, H. Seto, S. Matsuura, H. Yamashita, ACS Appl. Mater. Interfaces 4 (2012) 6635–6639.
[16] T. Kamegawa, S. Matsuura, H. Seto, H. Yamashita (Eds.), Angew. Chem. Int. 52 (2013) 916–919.
[17] P.G. Hoertz, D.W. Thompson, L.A. Friedman, G.J. Meyer, J. Am. Chem. Soc. 124 (2002) 9690–9691.
[18] N. Wang, L. Zhu, Y. Huang, Y. She, Y. Yu, H. Tang, J. Catal. 266 (2009) 199–206.
[19] S. Weng, Z. Pei, Z. Zheng, J. Hu, P. Liu, ACS Appl. Mater. Interfaces 5 (2013) 12380–12386.
[20] M.K. Nowotny, L.R. Sheppard, T. Bak, J. Nowotny, J. Phys. Chem. C 112 (2008) 5275–5300.
[21] M. Kong, Y. Li, X. Chen, T. Tian, P. Fang, F. Zheng, X. Zhao, J. Am. Chem. Soc. 133 (2011) 16414–16417.
[22] M. D'Arienzo, J. Carbajo, A. Bahamonde, M. Crippa, S. Polizzi, R. Scotti, L. Wahba, F. Morazzoni, J. Am. Chem. Soc. 133 (2011) 17652–17661.
[23] G. Kresse, J. Hafner, Phys. Rev. B 47 (1993) 558–561.
[24] G. Kresse, J. Furthmüller, Phys. Rev. B 54 (1996) 11169–11186.
[25] G. Kresse, J. Furthmüller, Phys. Rev. B 6 (1996) 15–50.
[26] J.P. Perdew, J.A. Chevary, Phys. Rev. B 46 (1992) 6671–6687.
[27] P.E. Blöchl, Phys. Rev. B 50 (1994) 17953–17979.
[28] G. Kresse, D. Joubert, Phys. Rev. B 59 (1999) 1758–1775.
[29] D.J. Chadi, M.L. Cohen, Phys. Rev. B 8 (1973) 5747–5753.
[30] W.L. Huang, J. Comput. Chem. 30 (2009) 1882–1891.
[31] H.-C. Chen, C.-W. Huang, J.C.S. Wu, S.-T. Lin, J. Phys. Chem. C 116 (2012) 7897–7903.
[32] A. Ramakrishnan, S. Neubert, B. Mei, J. Strunk, L. Wang, M. Bledowski, M. Muhler, R. Beranek, Chem. Commun. 48 (2012) 8556–8558.
[33] X. Pan, N. Zhang, X. Fu, Y.-J. Xu, Appl. Catal., A 453 (2013) 181–187.
[34] T. Hirakawa, H. Kominami, B. Ohtani, Y. Nosaka, J. Phys. Chem. B 105 (2001) 6993–6999.
[35] J. Zhuang, W. Dai, Q. Tian, Z. Li, L. Xie, J. Wang, P. Liu, X. Shi, D. Wang, Langmuir 26 (2010) 9686–9694.
[36] R. Li, H. Kobayashi, J. Guo, J. Fan, Chem. Commun. 47 (2011) 8584–8586.
[37] W. Ren, Z. Ai, F. Jia, L. Zhang, X. Fan, Z. Zou, Appl. Catal. B 69 (2007) 138–144.
[38] Z. Li, Y. Shen, C. Yang, Y. Lei, Y. Guan, Y. Lin, D. Liu, C.-W. Nan, J. Mater. Chem. A 1 (2013) 823–829.
[39] A.K. Chakraborty, S.B. Rawal, S.Y. Han, S.Y. Chai, W.I. Lee, Appl. Catal., A 407 (2011) 217–223.
[40] Z. Pei, L. Ding, J. Hu, S. Weng, Z. Zheng, M. Huang, P. Liu, Appl. Catal. B 142–143 (2013) 736–743.
[41] R. Ciriello, A. Guerrieri, F. Pavese, A.M. Salvi, Anal. Bioanal. Chem. 392 (2008) 913–926.
[42] K. Zhao, L. Zhang, J. Wang, Q. Li, W. He, J.J. Yin, J. Am. Chem. Soc. 135 (2013) 15750–15753.
[43] N. Zhang, Y. Zhang, X. Pan, X. Fu, S. Liu, Y.-J. Xu, J. Phys. Chem. C 115 (2011) 23501–23511.
[44] S. Sun, W. Wang, L. Zhang, J. Phys. Chem. C 117 (2013) 9113–9120.
[45] S. Qourzal, N. Barka, M. Tamimi, A. Assabbane, Y. Ait-Ichou, Appl. Catal. A 334 (2008) 386–393.
[46] J. Theurich, D.W. Bahnemann, R. Vogel, F.E. Ehamed, G. Alhakimi, I. Rajab, Res. Chem. Intermediat 23 (1997) 247–274.
[47] T. Hirakawa, Y. Nosaka, Langmuir 18 (2002) 3247–3254.